# SIMULATION OF TEMPERATURE FIELD AND OPTIMIZATION OF HEAT DISSIPATION STRUCTURE FOR LITHIUM-ION POWER BATTERY PACK BASED ON MULTI-OBJECTIVE FUNCTION OPTIMIZATION

by

***Feng LI****

Yellow River Conservancy Technical Institute, Kaifeng, Henan, China

Original scientific paper
https://doi.org/10.2298/TSCI2402263L

*In order to improve the thermal power dissipation of batteries and reduce the maximum temperature difference of batteries, the air conditioning system using battery type was optimized. Using multi-objective optimization method based on orthogonal experiment and multiple rotations, the local optimum values of multi-objective were obtained: the left end height A of entrance area and the height B of air outlet were 9 mm and 28 mm, respectively, with a tolerance value C of 0.4 mm for battery spacing. The simulation results of this optimization model show that the maximum temperature difference of the battery volume is 306.627 K (33.477 ℃) and 3.815 K (3.815 ℃), respectively. Compared with the initial model, they are reduced by 9.55% and 25.89%, respectively. Compared with the single factor analysis optimization model, they are reduced by 0.36% and 20.27%, respectively, indicating that the multi-objective optimization results are better. This multi- objective programming solves the problem of different parameters of air conditioning heat dissipation model to some extent, and can provide reference for the optimization design of other models.*

Key words: *lithium-ion power battery pack, temperature field simulation, optimization of heat dissipation structure, multi-objective function optimization*

## Introduction

With the intensification of environmental pollution, governments around the world strongly support the development of new energy vehicles to reduce their pollution the atmosphere. As a zero pollution vehicle model, pure electric vehicles have received attention from governments and major automobile companies around the world, investing a large amount of funds in research. Battery is the only energy source for pure electric vehicles, and is an important component of pure electric vehicles, it has always been a research hotspot [1]. For battery packs used in pure electric vehicles, due to the high demand for power and strict requirements for volume, a large number of battery cells will be stacked and arranged in a limited space, During operation, lithium-ion power batteries will release a lot of heat, resulting in a rapid increase in the temperature of the battery pack. Therefore, the problems of heat dissipation and temperature uniformity will become the focus. Therefore, it is necessary to adopt appropriate heat dissipation technique to provide a reasonable and stable heat environment for lithium-ion battery pack [2]. If there is no way to heat dissipation, it will not only affect the service life of

* Author's e-mail: fl_1142@163.com

the battery pack, but also thermal runaway and other situations may occur, which will lead to battery pack deflagration, explosion and other dangerous accidents seriously endangering the safety of passengers' lives and property. It can be seen that in order to provide a good working environment for lithium-ion batteries, a suitable battery thermal management system (BTMS) is needed. The BTMS is based on the influence of the external environmental temperature of the battery pack on the battery, integrating the heat generation mechanism and electrochemical performance of the battery, including materials science, electrochemistry, heat transfer and other engineering applications, it is a new technology to prevent thermal battery running out and improve battery performance, safety and life. Lithium-ion batteries have become an important power source for pure electric vehicles and hybrid electric vehicles because of their unique power, high power density, low pollution, low memory loss, and long life span. However, lithium-ion batteries produce a lot of heat during discharge, resulting in an increase in the internal temperature of the battery pack. Excessive working temperature can seriously affect the performance of battery packs, as well as the main parameters such as battery capacity, cycle life, and voltage index. For charging at low temperature, because the physical properties of electrode materials are too stable and the electrochemical reaction impedance increases, the polarization internal resistance increases rapidly, and the charging and discharging efficiency and capacity decrease sharply. Therefore, the normal operation of lithium-ion batteries requires a stable temperature range [3, 4].

In order to improve the thermal power dissipation of batteries and reduce the maximum temperature difference of batteries, the air conditioning system using battery type was optimized. Using multi-objective optimization method based on orthogonal experiment and multiple rotations, the local optimum values of multi-objective were obtained: the left end height A of entrance area and the height B of air outlet were 9 mm and 28 mm, respectively, with a tolerance value $C$ of 0.4 mm for battery spacing. The simulation results of this optimization model show that the maximum discharge temperature and the ignition temperature of the battery pack are 306.627 K (33.477 ℃) and 3.815 K (3.815 ℃), respectively. Compared with the initial model, they are reduced by 9.55% and 25.89%, respectively. Compared with the single factor analysis optimization model, they are reduced by 0.36% and 20.27%, respectively, indicating that the multi-objective optimization results are better. This multi-objective programming solves the problem of different parameters of air conditioning heat dissipation model to some extent, and can provide reference for the optimization design of other models.

## Model establishment and simulation

### *Establishment of initial geometric modelling of air cooling structure of lithium-ion battery pack*

The lithium metal phosphate cathode lithium-ion battery (developed in Dongguan) was selected as experimental battery,with a size of 16 mm × 65 mm × 131 mm, the Nameplate capacity is 10 Ah, and the nominal voltage is 3.2 V. The total size of the battery box is 230 mm × 73 mm × 175 mm, with wall thickness of 2 mm, the battery box has air inlet at the bottom of right and air outlet at the top. Ten individual batteries are arranged at equal intervals of 6 mm, with numbers 1-10 from right to left and air-flow channels 1-11. Import the geometric modelling into ICEMCFD software, and conduct unstructured grid division, and obtain about 750000 grids [5].

*Simulation settings*

The simulation experiment is set to discharge at a rate of 2*C* under steady-state heat transfer conditions, and the average heat generation rate of the battery is 20.993 kW/m$^3$, set as the internal heat source. The air temperature is 298.15 K (25 °C), the air inlet speed is 3 m/s, and convection heat transfer coefficient between air and the outer wall of the battery box is 5 W/m$^2$K. The energy balance, energy balance, equilibrium, and equilibrium equations all use the finite element method and the second upwind method. Thermophysical parameters of air, batteries, and containers are shown in tab. 1 [6].

**Table 1. Thermophysical parameters of air, battery, and box materials**

| Media name | $p$ [kgm$^{-3}$] | $C$ [Jkg$^{-1}$K$^{-1}$] | $k$ [Wm$^{-1}$K$^{-1}$] |
|---|---|---|---|
| Batery | 1958.81 | 733.1 | $kx$ =3.7, $ky$ = $kz$ = 10.9 |
| Air | 1.2261 | 1006.441 | 0.02421 |
| Batery box | 7930 | 500 | 16.3 |

*Simulation analysis*

By numerical calculation, the velocity distribution of the first water model in the area is obtained. The wind speed of Channel 1-3 is close to the inlet and outlet of the battery box, and the outlet is faster, while the wind speed of Channel 7-11 slows down the inlet and outlet of the battery box, causing air deformation. Air-flows from the bottom to the top and absorbs heat generated by batteries from the streams flowing between them. An increase in temperature results in an increase in flow resistance and heat transfer, resulting in a decrease in the heat capacity of the battery head over the bottom, resulting in a temperature difference between the two ends of a battery. The maximum temperature at the upper end of the battery pack is 2.4%, 5.8%, and 9% is 309.585 K (36.4359 °C), which is lower than 40 °C. The average temperature difference of the battery pack is 4.29 K (4.29 °C). Within the allowable temperature difference of 5 °C, the allowable temperature difference is good, but the maximum allowable temperature difference is 5.148 K (5.148 °C), which is 5 °C higher than the allowable temperature difference [7].

## Optimization of air cooling and heat dissipation structure for battery pack

According to the simulation results, the factors that affect the air cooling and heat dissipation effects of the battery pack mainly include the input area, the outlet, and the battery gap, as shown in fig. 1.

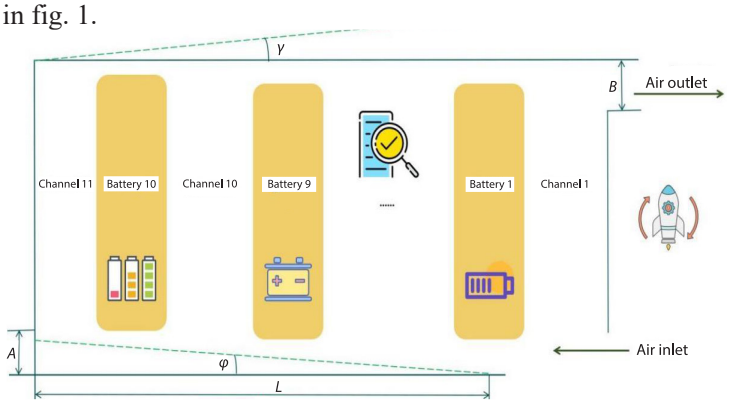


**Figure 1. Schematic diagram of air cooling and heat dissipation structure of battery pack**

The air inlet angle of the battery box is $\varphi$, when the size of the air inlet is unchanged, it can be changed by changing the size. To adjust the height A of the left end of the air inlet area. The outlet air angle of the battery box is $\gamma$. When the height of the left end of the upper air-flow channel remains unchanged,it can be changed by $\gamma$. To adjust the size of the air outlet pressure B [8]. The deviation of the battery is equal to the width of the air-flow channel, arranged in an equal and decreasing order from left to right, with a tolerance value of *C*. When the lateral dimension, *L*, of the battery box remains unchanged, changing the tolerance value *C* can adjust the battery spacing. The initial values of *A*, *B*, and *C* are 20 mm, 20 mm, and 0, respectively .

### *Orthogonal design of experiments*

In order to improve the heat dissipation ratio, reduce the temperature difference of the battery pack, and further reduce the maximum temperature, based on the analysis of the former, the effects of three configurations on the heat dissipation of the battery pack are comprehensively analyzed. Multi-objective optimization method based on orthogonal experiment was adopted. Three factors, *A*, *B*, and *C*, were selected for the orthogonal experiment, examining the first-order interaction between *A*, *B*, and *C*, $A \times B$, $B \times C$, and $A \times C$. Ignore secondary interaction $A \times B \times C$. Add the error term *D*, totaling seven columns. Construct an orthogonal experimental table L18 (37) with seven columns and three levels [9].

### *Multi-objective optimization*

The multi-objective optimization method that combines objective functions with constraint conditions is suitable for solving local optimal solutions with high accuracy and requires fewer iterations than genetic algorithms, improving computational efficiency.

Definitions of objective function and variational method:

$$\begin{gathered} \mathrm{Min}F(a,b,c) = \left[T_{\max}(a,b,c), \Delta T(a,b,c)\right] \\ 3 \le a \le 20 \\ 20 \le b \le 45 \\ 0 \le c \le 1 \end{gathered} \tag{1}$$

where $F(a, b, c)$ represents the objective function, $T_{mx}$ – the highest $T_{max}$ temperature of the battery pack, and $\Delta T$ – the temperature difference of the battery pack. The *a*, *B*, and *c* are design variables, representing the sizes of *A*, *B* and *C*. Seven discrete values are selected for each, as shown in tab. 2.

**Table 2. Design variables and discrete values**

| Design variable | Discrete value | | | | | | |
|---|---|---|---|---|---|---|---|
| | *a* | *b* | *c* | *d* | *e* | *f* | *g* |
| Size *A* | 3 | 5 | 8 | 9 | 10 | 15 | 20 |
| Size *B* | 20 | 25 | 28 | 30 | 35 | 40 | 45 |
| Tolerance value *C* | 0 | 0.2 | 0.4 | 0.5 | 0.6 | 0.8 | 1.0 |

Determine the selection rules for design variables and levels. In the initial design, if a certain discrete value is selected as the second level, then the discrete values adjacent to the second level are selected for the first and third levels. Referring to the results of the single factor analysis, set the initial value of the first iteration the *AdBdCd* combination in tab. 2, and use it as the second level, that is, dimension *A* is 9 mm, dimension *B* is 30 mm, and tolerance

value *C* is 0.5 mm. Select *AcBcCc* from tab. 2 for the first and third levels, respectively. Combination with *AeBeCe*. Starting from the second iteration, the second level of the initial value is taken as the optimal result of the previous iteration. By using the comprehensive weighting method and introducing weight coefficients, the originally defined multi-objective function is transformed into an equivalent single objective function. Then, the penalty function method is used to combine the constraint conditions with the equivalent single objective function modify the objective function value, making the results more accurate. The equivalent single objective function (characteristic function) expression:

$$CF = \omega_1 \frac{T_{\max 0}}{T_{\max}} + \omega_2 \frac{\Delta T_0}{\Delta T} \tag{2}$$

where *CF* is the characteristic function, $T_{\max 0}$, $\Delta T$, $T_{\max}$, and $\Delta T$ are the current values of the highest temperature and temperature difference of the battery pack, respectively, and $\omega_1$, $\omega_2$ – the weight coefficients of these two objective functions. Considering that both optimization objectives are equally important for evaluating the air cooling and heat dissipation effect of the battery pack, $\omega_1 = \omega_2 = 0.5$. From eq. (2), it can be seen that the smaller $T_{\max}$ and $\Delta T$, the greater *CF*, which objectively reflects the better air cooling heat dissipation effect .

### *Analysis of orthogonal test results*

Determine 18 experimental plans and establish corresponding simulation models for calculation. Use the same simulation settings and boundary conditions as the simulation experiment to obtain FLUENT simulation results. Use eq. (2) to calculate the *CF* values of the 18 models, and the results are listed in tab. 3.

**Table 3. The L18 (37) orthogonal test scheme and CF values**

| Number | $A_1$ | $B_2$ | $A \times B_3$ | $C_4$ | $A \times C_5$ | $B \times C_6$ | $D_7$ | *CF* |
|---|---|---|---|---|---|---|---|---|
| 1 | 1 | 1 | 1 | 1 | 1 | 1 | 1 | 0.9432 |
| 2 | 1 | 2 | 2 | 2 | 2 | 2 | 2 | 1.0309 |
| 3 | 1 | 3 | 3 | 3 | 3 | 3 | 3 | 1.0252 |
| 4 | 2 | 1 | 1 | 2 | 2 | 3 | 3 | 0.9622 |
| 5 | 2 | 2 | 2 | 3 | 3 | 1 | 1 | 1.1665 |
| 6 | 2 | 3 | 3 | 1 | 1 | 2 | 2 | 1.0359 |
| 7 | 3 | 1 | 2 | 1 | 3 | 2 | 3 | 0.9575 |
| 8 | 3 | 2 | 3 | 2 | 1 | 3 | 1 | 1.0411 |
| 9 | 3 | 3 | 1 | 3 | 2 | 1 | 2 | 1.1759 |
| 10 | 1 | 1 | 3 | 3 | 2 | 2 | 1 | 1.0534 |
| 11 | 1 | 2 | 1 | 1 | 3 | 3 | 2 | 0.9546 |
| 12 | 1 | 3 | 2 | 2 | 1 | 1 | 3 | 1.0462 |
| 13 | 2 | 1 | 2 | 3 | 1 | 3 | 2 | 1.0534 |
| 14 | 2 | 2 | 3 | 1 | 2 | 1 | 3 | 1.005 |
| 15 | 2 | 3 | 1 | 2 | 3 | 2 | 1 | 1.0463 |
| 16 | 3 | 1 | 3 | 2 | 3 | 1 | 2 | 0.9700 |
| 17 | 3 | 2 | 1 | 3 | 1 | 2 | 3 | 1.1720 |
| 18 | 3 | 3 | 2 | 1 | 2 | 3 | 1 | 1.0390 |

Using the characteristic function value as the index, perform a quantitative analysis of the orthogonal test in tab. 3. Add test values of each to get the maximum number of orthogonal tests for each, as shown in tab. 4.

**Table 4. Range analysis results**

| Index | $A_1$ | $B_2$ | $A \times B_3$ | $C_4$ | $A \times C_5$ | $B \times C_6$ | $D_7$ |
|---|---|---|---|---|---|---|---|
| $k_{1j}$ | 6.055 | 5.94 | 6.252 | 5.934 | 6.294 | 6.306 | 6.288 |
| $k_{2j}$ | 6.271 | 6.372 | 6.294 | 6.096 | 6.264 | 6.294 | 6.223 |
| $k_{3j}$ | 6.355 | 6.367 | 6.132 | 6.647 | 6.13 | 6.072 | 6.168 |
| $R_j$ | 0.3 | 0.432 | 0.162 | 0.714 | 0.174 | 0.234 | 0.13 |
| $S_j$ | 0.008 | 0.020 | 0.002 | 0.046 | 0.003 | 0.006 | 0.001 |

From tab. 4, it can be seen that the range $R$, in descending order, is $R4$, $R2$, $R1$, $R6$, $R5$, $R3$, and $R7$. Therefore, the primary and secondary order of the importance of the influence of the characteristic function values is $C$, $B$, $A$, $B \times C$, $A \times C$, $A \times B$, and $D$. The extremely small range value of error column $D$ indicates that the reliability of range analysis in this orthogonal experiment is high. Therefore, the optimal horizontal combination is determined as $A_3B_2C_3$, corresponding to the 17th scheme in tab. 3, which is size $A$ of 8 mm, size $B$ of 30 mm, and tolerance value $C$ of 0.4 mm.

In order to further investigate the significance of the impact of various factors on the experimental indicators, an analysis of variance was conducted on the simulation results in tab. 3. The results are shown in tab. 5.

**Table 5. Analysis of variance results**

| Source of variance | Sum of squared deviations, $S_j$ | Freedom, $f_j$ | Sum of mean squares, $s_j$ | $F_j$ | $Fa$ |
|---|---|---|---|---|---|
| $A$ | 0.008 | 2 | 0.004 | 8 | $F0.95(2, 2) = 19$ |
| $B$ | 0.020 | 2 | 0.010 | 20 | $F0.975(2, 2) = 39F0.95F0.95(2, 2) = 19$ |
| $C$ | 0.046 | 2 | 0.023 | 46 | $F0.99(2, 2) = 99F0.95F0.95(2, 2) = 19$ |
| $A \times B$ | 0.002 | 2 | 0.001 | 2 | $F0.95(2, 2)=19$ |
| $A \times C$ | 0.003 | 2 | 0.0015 | 3 | $F0.95(2, 2)=19$ |
| $B \times C$ | 0.006 | 2 | 0.003 | 6 | $F0.95(2, 2) = 19$ |
| $D$ | 0.001 | 2 | | | |

From tab. 5, it can be seen that since $FC$ and $FB$ are both more than $F0.95$ (2, 2), it shows that factors $C$ and $B$ have great influence on the maximum and temperature difference of the battery pack. It can also be seen that $A$ and $B \times C$ interactions have some but not significant effects, $A \times B$ and $A \times C$ interactions are very small.

### *Iteration and convergence of multi-objective optimization*

The optimal combination $A_3B_2C_3$ for the first iteration was determined using range analysis and variance analysis. Starting from the second iteration, select the optimal result of the previous iteration as the second level of the initial value for the next iteration. Using the method of continuous iteration, the local optimal solution for multi-objective optimization is

sought by continuously updating the 3-level orthogonal experimental table. If the results of the current iteration are the same as those of the previous iteration, that is, if the selected levels are the same, then the first and third levels will be the next optional values, adjacent to the second level in the next iteration.

Perform convergence tests on the optimal results obtained from each iteration. The convergence condition is:

– after three consecutive iterations, the characteristic function value will no longer increase,
– the total number of iterations is seven times the number of discrete values of the design variable; if the convergence condition is met, the iteration terminates, and
– if the conditions are not met, increase the number of iterations until convergence.

After multiple iterations, the iterative process curve of multi-objective optimization based on orthogonal experiments was obtained, as shown in fig. 2. Combining the convergence conditions, it is determined that the iterative process converges, so the multi-objective optimization results are reliable.

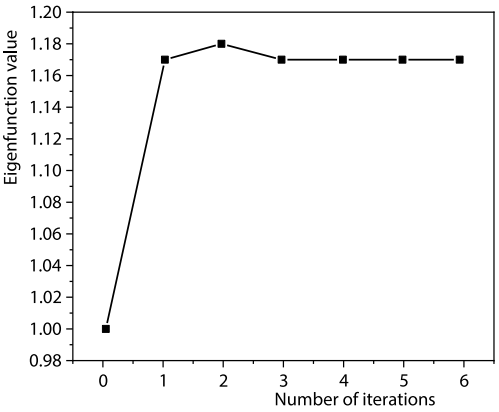


**Figure 2. Iterative process curve of multi-objective optimization**

### *Comparison of optimization results*

After six iterations, the iterative process converged and the multi-objective optimization local optimal solutions for $A$ and $B$ were 306.627 K (33.477 °C) and 3.815 K (3.815 °C), respectively. The corresponding dimensions of the air-cooled structure model in fig. 2 are: $A$ = 9 mm, $B$ = 28 mm, and $C$ = 0.4 mm. The comparison results between the multi-objective optimization model, the initial model, and the single factor analysis optimization model are shown in tab. 6.

**Table 6. Comparison of multi-objective optimization model with initial model and single factor analysis optimization model**

| Structural model | $A$ [mm] | $B$ [mm] | $C$ [mm] | $T_{max}$ [K] | $\Delta T$ [K] |
|---|---|---|---|---|---|
| Initial model | 20 | 20 | 0 | 309. 586 | 5. 149 |
| Single factor analysis optimization model | 8 | 30 | 0. 5 | 307. 727 | 4. 786 |
| Multi-objective optimization model | 9 | 28 | 0. 4 | 306. 628 | 3. 816 |

From tab. 6, it can be seen that compared with the initial model, the multi-objective optimization model has reduced $T_{max}$ and $\Delta T$ by 9.55% and 25.89%, respectively. Compared with the single factor analysis optimization model, the multi-objective optimization model has reduced $T_{max}$ and $\Delta T$ by 0.36% and 20.27%, respectively. The multi-objective optimization model has better air cooling and heat dissipation effect [10].

## Conclusion

Set the target temperature dissipation a maximum temperature not exceeding 40 °C and the temperature not exceeding 5 °C. The first geometric model of air conditioning system of battery pack was established. Considering the effects of three factors of heat dissipation, such

as entry angle, outlet angle and battery spacing, orthogonal experiments were designed to find out the optimum process for air conditioning heat dissipation model of battery packs. The basic model of air conditioning system of lithium-ion battery pack was established, and the temperature field and flow field were simulated using the CFD theory and FLUENT software. Based on the simulation results, considering the three kinds of inlet angle, outlet angle and battery spacing, multi-objective optimization method was achieved according to orthogonal experiment and proposed an optimization method. In order to minimize the maximum temperature difference between battery packs, a local solution was obtained by several measures: the left side height of the intake port was 9 mm (the intake angle was 2.74), and the outlet height was 28 mm (outlet angle 2), and the battery's differential protection cost is 0.4 mm. Compared with the original design, the improved design reduces the maximum battery volume by 9.55% and the temperature difference by 25.89%.

## References

[1] Wang, Y., *el al*., Liquid-Cooled Cold Plate for a Li-Ion Battery Thermal Management System Designed by Topology Optimization, *Journal of Mechanical Science and Technology*, *37* (2023), 4, pp. 2079-2086
[2] Hu, Y., Bidirectional Analysis Model of Green Investment and Carbon Emission Based on LSTM Neural Network, *Thermal Science*, *27* (2023), 2B, pp. 1405-1415
[3] Sheng, L., *el al*., Non-Linear Dynamics Analysis of Gear Transmission System Considering Tooth Surface Friction and Thermal Deformation, Proceedings of the Institution of Mechanical Engineers – Part K: *Journal of Multi-body Dynamic*s, *237* (2023), 2, pp. 220-235
[4] Li, Y., *el al*., Optimization of Charging Strategy for Lithium-Ion Battery Packs Based oon Complete Battery Pack Model, *The Journal of Energy Storage*, *37* (2021), 9, pp. 102466
[5] Xu, H., *el al*., Optimization of Liquid Cooling and Heat Dissipation System of Lithium-Ion Battery Packs of Automobile, *Case Studies in Thermal Engineering*, *2*6 (2021), 1, 101012
[6] Pizarro-Carmona, V., *et al*., Ga-Based Approach to Optimize an Equivalent Electric Circuit Model of a Li-Ion Battery-Pack, *Expert Systems with Applications*, *172* (2021), 8, 14647
[7] Wan, C., Tssr Algorithm Based Battery Space Optimization on Thermal Management System, *International Journal of Green Energy*, *18* (2021), 12, pp. 1203-1218
[8] Li, D., *et al*., Investigation of the Explosion Characteristics of Ethylene-Air Premixed Gas in Flame Proof Enclosures by Using Numerical Simulations, *Thermal Science*, *27* (2023), 2B, pp. 1573-1586
[9] Li, Y., Guo, S., Material Design and Structure Optimization for Rechargeable Lithium-Sulfur Batteries, *Matter*, *4* (2021), 4, pp. 1142-1188
[10] Feng, X., Reliability Optimization Design of Intelligent Mechanical Structure for Waste Heat Recovery, *Thermal Science*, 27 (2023), 2A, pp. 1083-1090

Paper submitted: May 11, 2023
Paper revised: July 22, 2023
Paper accepted: September 1, 2023